Original Research Article

OPEN ACCESS

The PPAR-gamma agonist pioglitazone alleviates bleomycin-induced lung fibrosis in male BALB/c mice

Alina Kabaliei, Vitalina Palchyk, Olga Izmailova, Viktoriya Shynkevych, Oksana Shlykova, and Igor Kaidashev

Poltava State Medical University, Poltava, Ukraine

ABSTRACT

Background: Many transcription factors may be involved in the pathogenesis of pulmonary fibrosis (PF). One such factor is PPARG. The PPARG agonist, pioglitazone (PG), has demonstrated general lung protective activity in animal models and is considered a promising therapeutic agent for fibrotic intervention. This study aimed to investigate the effect of PG on the expression of connective tissue remodeling genes in the lungs using bleomycin (BLM)-induced lung fibrosis (BIF).

Methods: The study was conducted on male BALB/c mice. PF was induced by pretreatment with bleomycin sulfate and cyclophosphamide. The mice were randomly divided into 3 groups: the first group was administered BLM at a dose of 0.15 U/kg in 50 µl of sterile saline (0.9% NaCl), and the second group was administered 50 µl of saline. The third group was not induced with pulmonary fibrosis and served as a control group. On the 4th day of the experiment, animals from the first and second groups were randomly divided into animals that received PG orally at a dose of 20 mg/kg or saline (40 µl) for 14 days. 4-hydroxyproline was determined in right lung tissue samples. Gene expression was determined using real-time PCR.

Results: PG administration to BIF mice resulted in a significant reduction and normalization of the total number of BAL cells, fibrosis score, mRNA expression of genes associated with connective tissue – *Col1a1* (P=0.0466), *Col3a1* (P=0.0053), *Mmp2* (P=0.0006), *Tgfb2* (P=0.0459), and *Tgfb3* (P=0.0017), as well as mRNA of genes regulating lung connective tissue inflammation and fibrosis – *Mrc1* (P=0.0263), *Edn1* (P=0.0012), *Pparg* (P=0.0044), *Nr1d1* (P=0.0053) and *Fn1* (P=0.0125).

Conclusions: PPARG activation by PG alleviates BIF by decreasing collagen deposition, *Col1a1* and *Col3a1* mRNA expression, remodeling of lung tissue (decreasing *Mmp2*, *Edn1*, and *Fn1* mRNA), and M2-specific profibrotic macrophage *Mrc1* mRNA.

Key words: pulmonary fibrosis, inflammation, bleomycin, pioglitazone, PPARG.

Correspondence: Igor Kaidashev, MD, 36011, Ukraine, Poltava, 23 Shevchenko Street, Poltava State Medical University - Phone: +380532629924 - E-mail: i.kaidashev@pdmu.edu.ua

Authors' contributions: Alina Kabaliei: investigation, visualization, statistical analysis; Vitalina Palchyk: investigation, visualization; Olga Izmailova: investigation, methodology, data curation, statistical analysis; Viktoriya Shynkevych: investigation, visualization, statistical analysis, writing – original draft; Oksana Shlykova: investigation, methodology, visualization; Igor Kaidashev: project administration, methodology, data curation, visualization, writing – original draft, and review & editing.

Ethics approval and consent to participate: This study was performed in line with the principles of the Declaration of Helsinki. Ethical approval and consent to participate in the study were obtained from the Committee on Bioethics and Ethical Issues of Poltava State Medical University (Minutes No. 207 as of 23.08.2022).

Consent for publication: Not applicable.

Availability of data and material: The data that support the findings of this study are available from the corresponding author upon reasonable request.

Conflict of interest: The authors declare no conflicts of interest.

Funding: The study was part of research project no. 0126U000355 «Development of new methods for diagnosis and personalized treatment of respiratory and comorbid diseases during wartime and post-war periods», funded by the Ministry of Healthcare of Ukraine.

Acknowledgements: Not applicable.

Introduction

Pulmonary fibrosis (PF) is a common complication of various lung diseases, including chronic obstructive pulmonary disease [1], bronchial asthma [2], COVID-19 infection [3], idiopathic PF [4], etc., and inhalation of aggressive substances such as silica [5], CO, NO_2, O_3, SO_2 [6], and tobacco smoking [7], etc. Severe PF may require lung or lung cell transplantation [8, 9].

The key factors of lung fibrosis are increased endothelial cell activation, dysfunctional vascular barrier integrity [10], excessive fibrillar collagen deposition in the interstitial extracellular matrix [11], impaired macrophage-fibroblast crosstalk [12], extracellular matrix dysregulation [13], and immune inflammation [14]. Many transcriptional factors might be involved in the promotion of lung fibrosis, such as Nf-κB [15], AP-1 [16], STAT3, FOXP1, JUNB, ATF3, FosL2, BATF, and Fra2 [17]. Other transcriptional factors, such as PPAR [18], Kruppel-like factor 2, CEBPA [19], NRF2F2 [20], etc., inhibited lung tissue fibrosis, counteracting profibrogenic factors.

PPARG investigations provided promising results to attenuate PF [21-24] using a PPARG agonist. One of the PPARG agonists, PG, demonstrated common lung protective activity in animal models of acute lung injury [25], pulmonary hypertension, right heart failure [26], hyperoxia-induced lung injury [27], sepsis-induced acute lung injury [28], and alcohol-induced alveolar macrophage phagocytic dysfunction [29], etc. Recently, it was shown that PG might be a potential therapeutic agent for fibrotic intervention [30].

This study assessed the effects of PG on the expression of connective tissue remodeling genes in murine lungs using BIF.

Material and Methods

Animals and experimental protocol

Four- to 8-week-old BALB/c male mice (n=56) were used throughout the study. Mice were kept at an ambient temperature 20±2°C under a 12h normal phase light-dark cycle and fed a standard diet. Drinking water and food were freely available.

The animal experiment was approved by the Commission on Bioethics and Ethical Issues of Poltava State Medical University (Protocol No. 207 of 23.08.2022).

In the study model, pulmonary fibrosis was induced with bleomycin sulfate in male BALB/c mice with pretreatment with cyclophosphamide to increase the fibrotic response by suppressing T-suppressor T cells, which modulate pulmonary fibrosis *in vivo* in BALB/c mice. For this purpose, 56 male mice were intraperitoneally injected with cyclophosphamide (Endoxan) (Baxter Oncology GmbH, Germany) at a dose of 100 mg/kg two days before BLM instillation. After treatment with cyclophosphamide, mice were randomly divided into 3 groups: the first group (BLM) (n=30) was administered BLM (Sigma-Aldrich, USA, Cat. No. 971) at a dose of 0.15 U/kg in 50 μl of sterile saline (0.9% NaCl) by oropharyngeal aspiration (OA) [31, 32]. The second group of animals (Saline) (n=20) received OA saline 50 μl. Before OA, as described previously, animals were lightly anesthetized with sodium thiopental (50 mg/kg) administered intraperitoneally [33]. The third group (n=6) was not exposed to the induction of pulmonary fibrosis and served as a control group.

After a single OA administration of BLM and saline, on day 4 of the experiment, animals of the first and second groups were randomly divided into animals receiving oral PG at a dose of 20 mg/kg, which was dissolved in sterile saline immediately before administration (40 μl) [34] or saline (40 μL) for n=15 and n=10 animals, respectively, for the first and second groups (hereinafter referred to as BLM + PG, BLM + Saline, and Saline + PG, Saline + Saline, respectively) for 14 days (Figure 1). On day 24 of the experiment, the animals were euthanized by intraperitoneal injection of sodium thiopental at a dose of 250 mg/kg, and the lungs were removed for further biochemical, histopathological, and molecular biological analyses.

Determination of 4-hydroxyproline in lung tissue samples

The right lung lobe samples were weighed, dried in an oven at 90°C, and the weight was recorded again. The weight loss coefficient in mice during the study period was calculated as the ratio of the initial weight

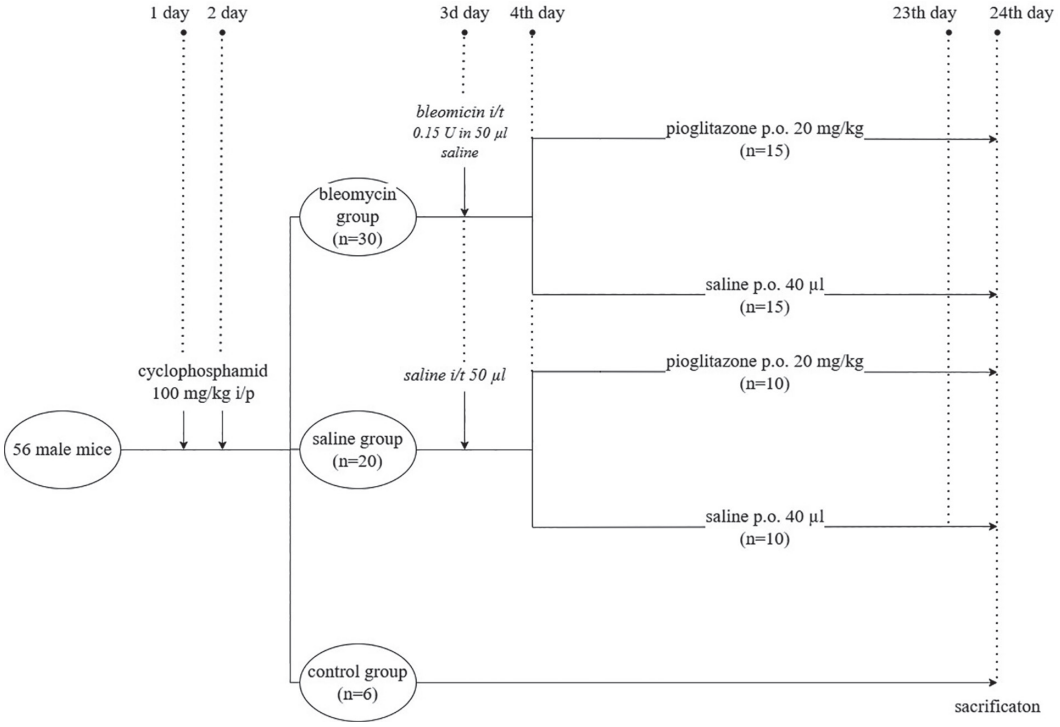

Figure 1. Research design.

of the mouse to its final weight. Dry tissues were placed in glass ampules containing 0.5 ml of 6M HCl (Sigma-Aldrich, USA, Cat. No. H1758) and soldered. Ampules were boiled at 120˚C for 8 hours. After cooling down and adding 5 µl of phenolphthalein (1%, Sigma-Aldrich, USA, Cat. No. 77098), the samples were neutralized with NaOH 10M (Sigma-Aldrich, USA, Cat.No. 1310732). Dark precipitate and brown color were removed by adding 100 µl of carbon suspension (10 mg/ml activated charcoal, Sigma-Aldrich, USA, Cat. No. 7440440) with further centrifugation. 5µl of standard or hydrolyzed sample were pipetted in duplicates onto 96 well plate, and 5 µl citrate acetate buffer (5% citric acid (Sigma-Aldrich, USA, Cat. No. 77929), 7.2% sodium acetate (Sigma-Aldrich, USA, Cat. No. 127093), 3.4% sodium hydroxide, 1.2% glacial acetic acid (Sigma-Aldrich, USA, Cat. No. 64197) was added to each well, as 100 µl of freshly prepared chloramine-T solution (14.1 mg Chloramine-T (Sigma-Aldrich, USA, Cat. No. 7080504), 100 µl n-propanol (Sigma-Aldrich, USA, Cat. No. 102603), 100 µl distilled water, 0.8 ml citrate acetate buffer). The samples were incubated at room temperature for 20 minutes. After adding 100 µl of Ehrlich's reagent (2.5 g of 4-(dimethylamino)benzaldehyde (Sigma-Aldrich, USA, Cat. No. 102603), 9.3 ml of n-propanol, and 3.9 ml of 70% perchloric acid (Carl Roth, Germany, Cat. No. 7601903), the plate was incubated for 20 minutes at 65˚C. After cooling down, the samples were measured at 492 nm on a LabLine-026 (Labline, Austria) photometer, and a standard curve from 0 to 3 mg/ml 4-hydroxyproline (Sigma-Aldrich, USA, Cat. No. 51354) was created. Data were expressed as µg/right lung lobe [32].

Bronchoalveolar lavage

Bronchoalveolar lavage (BAL) was performed according to the basic method [35]. Mice were euthanized with thiopental sodium, after which their chest cavities were opened and their left lungs were cannulated through the trachea. The left lungs were washed *in situ* with three consecutive aliquots of sterile 1× PBS, depending on the size of the mouse. The

wash fluid from one mouse was then collected, centrifuged at 1500 rpm for 10 minutes, and the cell pellet was resuspended in phosphate-buffered saline (PBS). To count the total number of cells in BAL, a standard method was used involving the vital dye trypan blue and a hemocytometer [36].

RNA preparation and quantitative reverse transcription PCR

Mice from all experimental and control groups were used for RNA extraction. Samples were collected from the caudal part of the left lung. Total RNA was extracted from the lung using the RNeasy mini kit (QIAGEN, Germany, Cat. No. 74104). To generate single-stranded DNAs, total RNA (≈1 μg, MaestroNano Spectrophotometer MN-913, Taiwan) was reverse transcribed using QuantiTect® Reverse Transcription Kit (QIAGEN, Germany, Cat. No. 205313). For SYBR Green-based analysis, the cDNA equivalent of 50 ng of total RNA from each sample was amplified in the CFX96TM Real-Time PCR Detection system (Bio-Rad, USA) using a QuantiTect® SYBR-green PCR Kit (QIAGEN, Germany, Cat. No. 204143).

The gene expressions were detectable as $2^{-\Delta Ct}$. All values were normalized to the expression of the housekeeping gene S2 [37].

The sequences of specific primers used for real-time PCR are provided in Table 1. All oligonucleotides were obtained from Metabion International AG (Germany).

All pairs of primers were checked for specificity by Primer-BLAST software (https://www.ncbi.nlm.nih.gov/tools/primer-blast/index.cgi), and PCR products were verified by the automatic capillary electrophoresis system QIAxcel Advanced (QIAGEN, Germany).

Histological analysis

For histopathological analysis, the middle 1/3 of the left lobe of each animal's lung was excised and inflated with 10% neutral buffered formalin immediately after sacrifice. Tissue samples were paraffin-embedded, and 3 μm-thick sections were stained with Mallory's trichrome (Abcam, Cat. No. 150686), which highlights collagen fibers in varying intensities of blue. Digital images were acquired using an Axiocam 105 Color camera mounted on an Axio Lab.A1 light microscope (Carl Zeiss, Göttingen, Germany) and processed using ZEN 2.5 Lite software (Blue edition, version V1.0 ru 04/2018 103).

An experienced pathologist, familiar with the study groups, assessed the level of fibrosis, defined as the presence of collagen structures, in all lung sections using a semiquantitative approach. Five areas of view were evaluated per tissue section using pixel-by-pixel analysis (pixel size: 2.2 × 2.2 μm), followed by the calculation of the ratio of the collagen-stained area to the total lung tissue area, referred to as the quantitative fibrosis coefficient. Image analysis was conducted using ImageJ open-source software. Staining vectors for collagen-rich areas were determined manually based on color information and the spatial localization of tissue structures.

To assess the reproducibility of collagen quantification, 12 measurements were conducted on 6 pairs of consecutive lung tissue sections stained using Mallory's trichrome method across different staining batches, following the protocol outlined by Masugi et al. [43].

Statistical analysis

Descriptive statistics was applied to the data using the GrafPad Prism version 8.0.1 for Windows statistical software package (GraphPad Prism Software, USA). Determination of the correspondence of quantitative indicators of the Gaussian distribution in groups was carried out using the D'Agostino-Pearson normality test. In the case of a normal distribution, the parametric statistics one-way ANOVA was used for multiple comparisons with subsequent testing of statistical hypotheses for pairwise comparisons using the Tukey test. If it was impossible to determine the normality of the distribution due to the small size of the group, calculations were performed using the non-parametric statistics Kruskal-Wallis test. The data on the graphs were presented as scatter plots of individual values, boxes with lines of the mean and standard deviation (M±SD) and violin plot for each of the studied groups. The study was based on the null hypothesis that administration of BLM, PG, or saline solution does not lead to changes in lung fibrosis or mRNA

Table 1. Primer sequences for mRNA measurement.

Gene	Primer sequences	Oligo ID	References
Mrc1	Forward: GTGGAGTGATGGAACCCCAG	230111B085A01 1/52	[38]
	Reverse: CTGTCCGCCCAGTATCCATC	230111B085B01 2/52	
Col1a1	Forward: CTGACGCATGGCCAAGAAGA	230111B085A02 9/52	[39]
	Reverse: ATACCTCGGGTTTCCACGTC	230111B085B02 10/52	
Col3a1	Forward: GGTGGTTTTCAGTTCAGCTATGG	230111B085C02 11/52	
	Reverse: CTGGAAAGAAGTCTGAGGAATG	230111B085D02 12/52	
Edn1	Forward: CCACAGACCAGGCAGTTAGAT	230111B085E02 13/52	
	Reverse: TGAATGGTACTTTGGGCCCTGA	230111B085F02 14/52	
Fn1	Forward: TCCAGCCCCACCCTACAAGT	230111B085A03 17/52	
	Reverse: CCAGACCAAACCATAAGAAC	230111B085B03 18/52	
Mmp2	Forward: TCAACGGTCGGGAATACAGC	230111B085E01 5/52	[40]
	Reverse: AGCTGTTGTAGGAGGTGCCCT	230111B085F01 6/52	
Mmp9	Forward: AAGGGTACAGCCTGTTCCTGGT	230111B085G01 7/52	
	Reverse: CTGGATGCCGTCTATGTCGTCT	230111B085H01 8/52	
Pparg	Forward: CCAGAGCATGGTGCCTTCGCT	211116B056G04 31/87	[41]
	Reverse: CAGCAACCATTGGGTCAGCTC	211116B056H04 32/87	
Tgfb2	Forward: CAGGAGTGGCTTCACCACAAAG	230111B085E03 21/52	[37]
	Reverse: TGGCATATGTAGAGGTGCCATCA	230111B085F03 22/52	
Tgfb3	Forward: TCGACATGATCCAGGGACTG	230111B085G03 23/52	
	Reverse: CCACTGAGGACACATTGAAACG	230111B085H03 24/52	
Nr1d1	Forward: CGTTCGCATCAATCGCAACC	191115B025G10 164/193	[42]
	Reverse: GATGTGGAGTAGGTGAGGTC	191115B025G06 132/193	
S2	Forward: TGCCAGTGCAGAAGCAGACT	230111B085A04 25/52	[37]
	Reverse: CACCAAGACCAACGTGACCA	230111B085B04 26/52	

expression in mouse lung tissue. P-values of <0.05 were considered statistically significant.

Results

Changes in 4-Hydroxyprolin and BAL Cellularity After BIF and PG Treatment in the Mouse Lung

We did not find any statistically significant differences in 4-Hydroxyprolin concentration in lung tissue, either after BIF or PG treatment (Figure 2A). We observed a significant increase in the total cell count in BAL in mice after BLM oropharyngeal instillation (*P*=0.0061). PG treatment of mice with BIF led to a significant decrease and normalization of the total cell count in BAL (*P*=0.0196) (Figure 2B). We have noted statistically significant differences in mice weight loss ratio after BLM oropharyngeal instillation (*P*=0,0029) (Figure 2C).

The changes in mouse lung morphology after BIF and PG treatment

The BIF development induced a significant increase in the fibrosis coefficient in the lung compared with control (*P*=0.0033), Saline + Saline (*P*=0.006), and Saline + PG (*P*=0.0001) groups (Figure 3A). PG treatment significantly decreased the fibrosis coefficient in comparison with BIF mice (*P*=0.0041).

Pathohistological scores in the main experimental group (BLM + PG) showed significant alleviation of BIF (Figure 3). In this group, the level of fibrosis did not significantly differ from that of the comparison groups: Saline + PG, Saline + Saline, or control.

In the BLM + Saline group, fibrosis scores reached the highest levels compared with all other groups, confirming the development of bleomycin-induced lung pathology.

The control and comparison groups – comprising mice treated with saline alone, saline administered twice, or PG combined with saline – showed no statistically significant differences in collagen deposition. All groups demonstrated normal lung architecture across all examined sections.

Changes in Col1a1, Col3a1, Mmp2, Mmp9, Tgfb2, and Tgfb3 mRNA after BIF and PG Treatment in the Mouse Lung

The levels of connective tissue-related genes' mRNA during BIF and after PG administration are shown in Figure 4. Treatment of control mice with oropharyngeal or oral saline and PG did not induce any significant changes in the mRNA expression of all investigation genes. The development of BIF significantly increased mRNA of *Col1a1* in comparison with control mice (*P*=0.0052); *Col3a1* – with control and saline-treated mice (*P*=0.0015, *P*=0.0030, respectively); *Mmp2* – with saline-treated mice (*P*=0.0373). At the same time, we observed a statistically insignificant increase in the mRNA expression of *Mmp9*, *Tgfb2*, and *Tgfb3* genes. PG treatment of BIF mice significantly decreased the mRNA expression of *Col1a1* (*P*=0.0466), *Col3a1* (*P*=0.0053), *Mmp2* (*P*=0.0006), *Tgfb2* (*P*=0.0459), *Tgfb3* (*P*=0.0017), and insignificantly decreased *Mmp9*.

Changes in Mrc1, Edn1, Pparg, Nr1d1, and Fn1 mRNA after BIF and PG treatment in the mouse lung

Figure 5 shows the mRNA expression of some genes that can regulate connective tissue inflammation and fibrosis in lung tissue. Control mice treated with oropharyngeal or oral saline and PG did not exhibit significant changes in the mRNA levels of the investigated genes. Fibrosis induced by BLM led to an increase in mRNA expression for *Mrc1* compared with control (*P*=0.0007) and saline-treated (*P*=0.0166) mice; Edn1 compared with saline-treated mice (*P*=0.0458); and *Fn1* compared with control mice (*P*=0.0205). *Pparg* and *Nr1d1* showed an insignificant increase in mRNA levels.

PG administration to BIF mice revealed a statistically significant decrease in *Mrc1* (*P*=0.0263), *Edn1* (*P*=0.0012), *Pparg* (*P*=0.0044), *Nr1d1* (*P*=0.0053), and *Fn1* (*P*=0.0125) mRNA.

Discussion

For the study of PG antifibrotic activity in the mouse lung, the model of BIF was used, following the

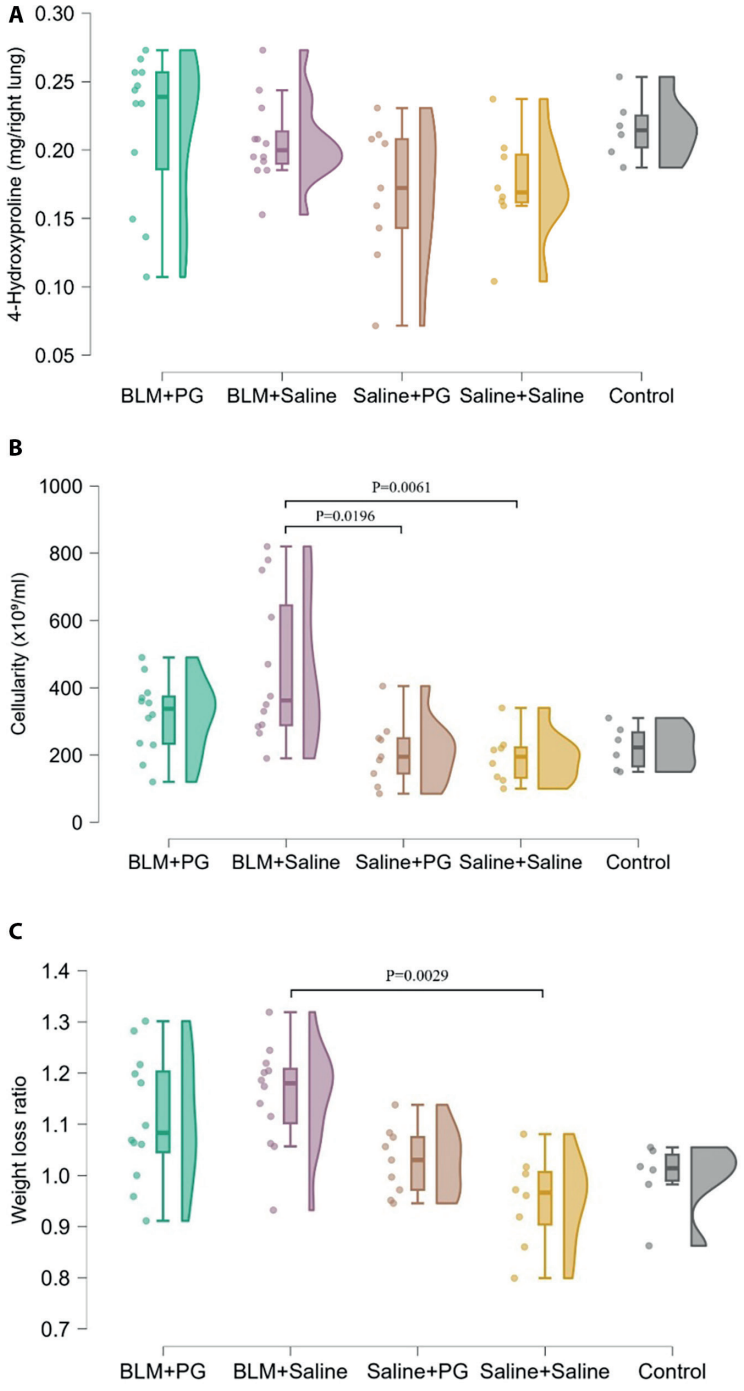

Figure 2. Changes in oxyproline content morphometric parameters in mouse lung tissue after the administration of pioglitazone during experimental inflammatory pulmonary fibrosis: A) 4-hydroxyproline/right lung; B) cellularity of bronchoalveolar lavage; C) weight loss ratio. Between-group differences were determined by one-way ANOVA with Tukey's *post hoc* test. The Kruskal-Wallis test was used to compare the Control group with all others. Exact P-values are given.

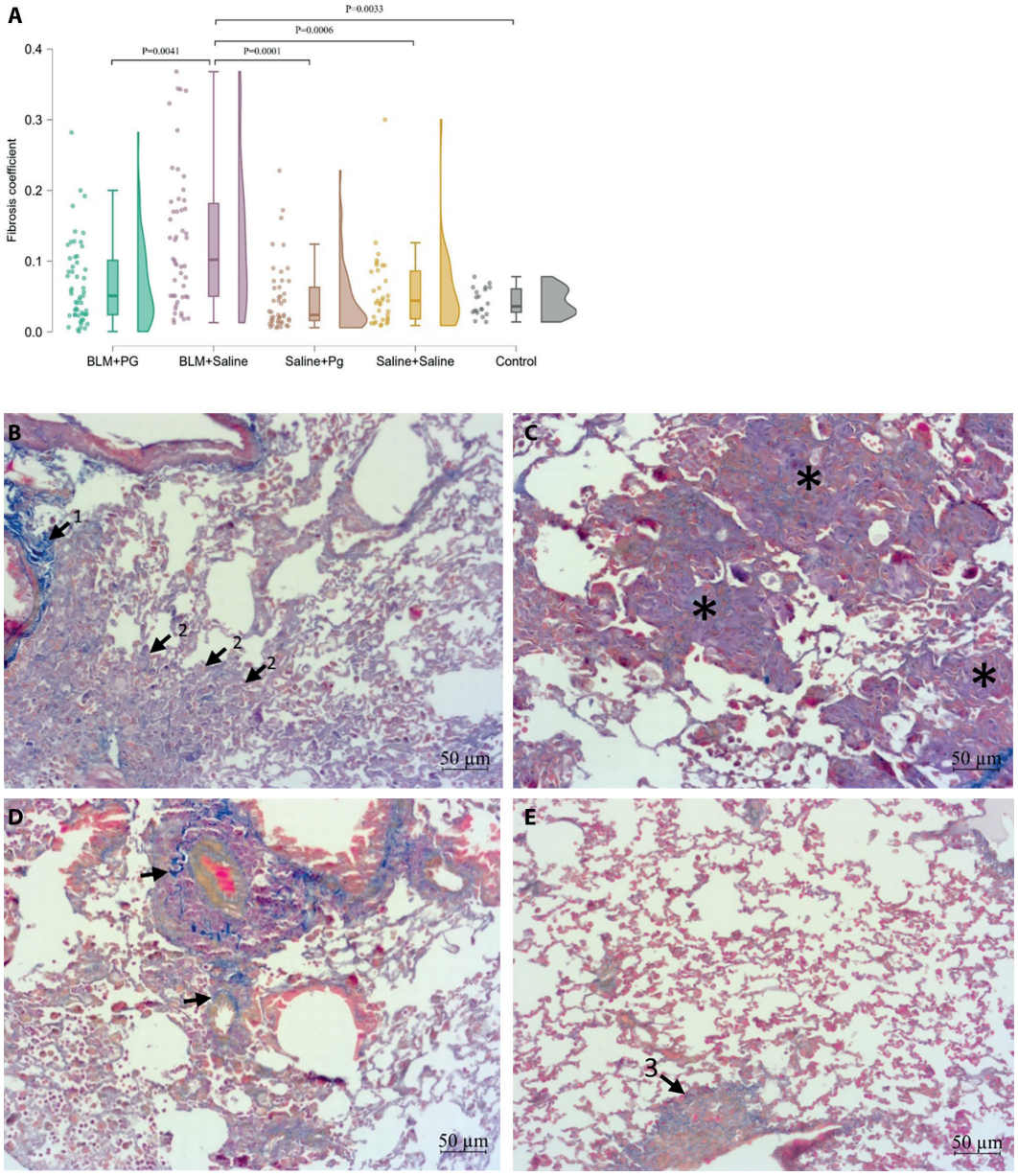

Figure 3. Lung tissue changes after the administration of PG during experimental PF (Mallory's trichrome staining). Scale bars 50 µm. A) changes of fibrosis coefficient in the lung of investigated groups. Representative histological section demonstrating collagen depositions in mouse lungs: B) decreased fibrosis persisting along the bronchovascular bundles following PG administration (1 – physiological collagen deposition; 2 – area of fibrotic changes in lung tissue (BLM + PG group); C) increased fibrosis spread from the bronchovascular bundles. Asterisks indicate areas of fibrotic changes in the lung tissue (BLM + Saline group); D) collagen structures of the lung appear normal along the bronchovascular bundles (arrows) in Saline + PG (comparison group); E) area of potential lung tissue fibrosis (Saline + Saline group). Between-group comparisons were performed using one-way ANOVA with Tukey's *post hoc* test. Exact P-values are given.

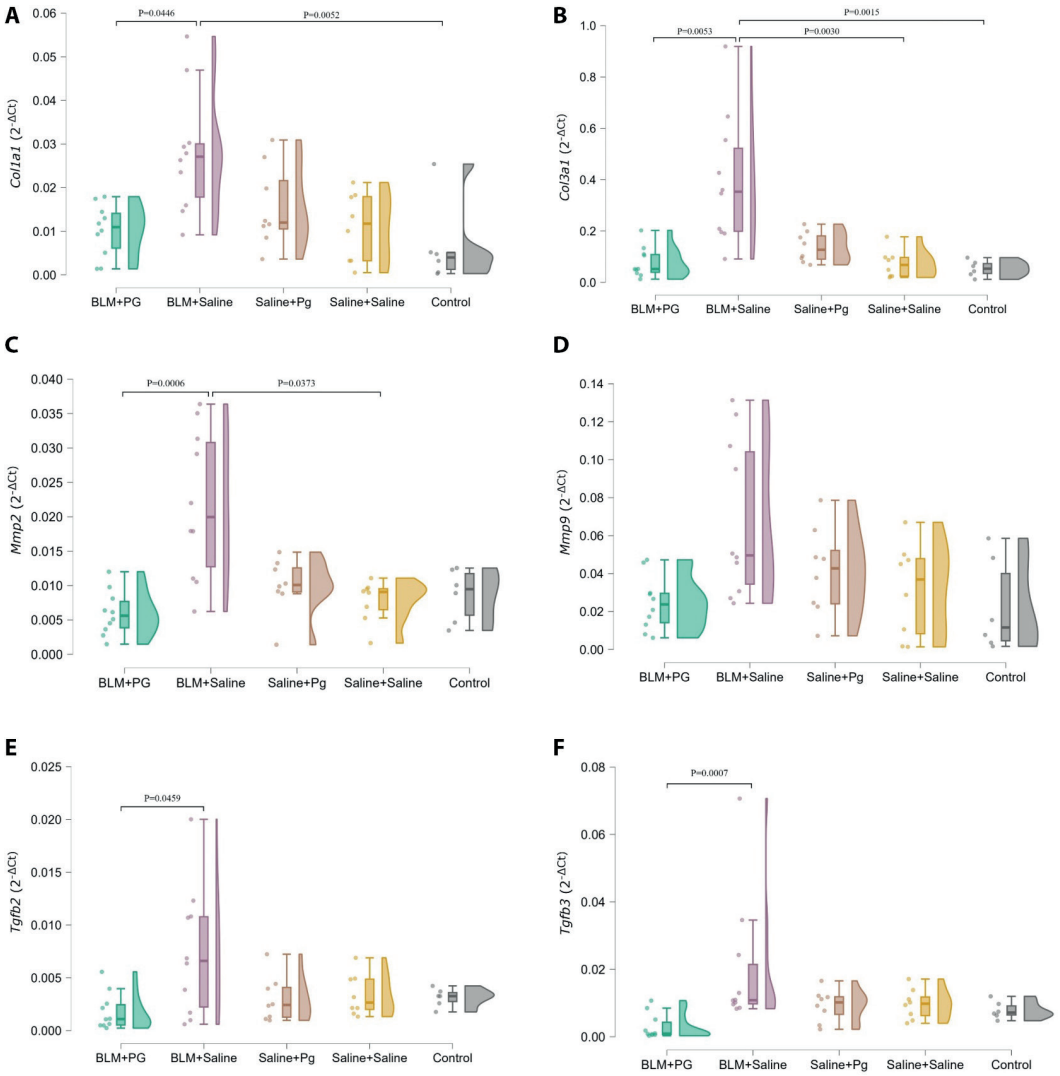

Figure 4. Changes in gene expression levels: A) *Col1a1*; B) *Col3a1*; C) *Mmp2*; D) *Mmp9*; E) *Tgfb2*; F) *Tgfb3*. Between-group differences were determined by one-way ANOVA with Tukey's *post hoc* test. The Kruskal-Wallis test was used to compare the Control group with all others. Exact P-values are given.

inhibition of cyclophosphamide-sensitive T cells [31]. This model produced the highest collagen synthesis in the lung 21 days after BLM administration. PG was administered for 20 days after BLM installation, and this time course was optimal for the investigation of its antifibrotic activity [44, 45].

Induction of BIF led to the increase of BAL total cellularity and lung hydratation. At the same time, during the pathomorphological examination, fibrosis coefficient increased significantly. These data were accompanied by an increase in *Col1a1* and *Col3a1* genes expression, and *Mmp2* gene expression.

COL1A1, a member of the collagen family involved in epithelial-mesenchymal transition [46], might serve as a fibrotic progression marker [47]. Similar properties were described for COL3A1 [48], and this protein might act synergistically with COL1A1 [49]. These findings suggest the development of lung fibrosis and collagen over-deposition. Although collagen over-deposition is a hallmark of lung fibrosis, current research mostly focuses on the cellular aspect, leaving collagen, particularly its dynamic remodeling (degradation and turnover), largely unexplored [50]. We did not observe statistically significant

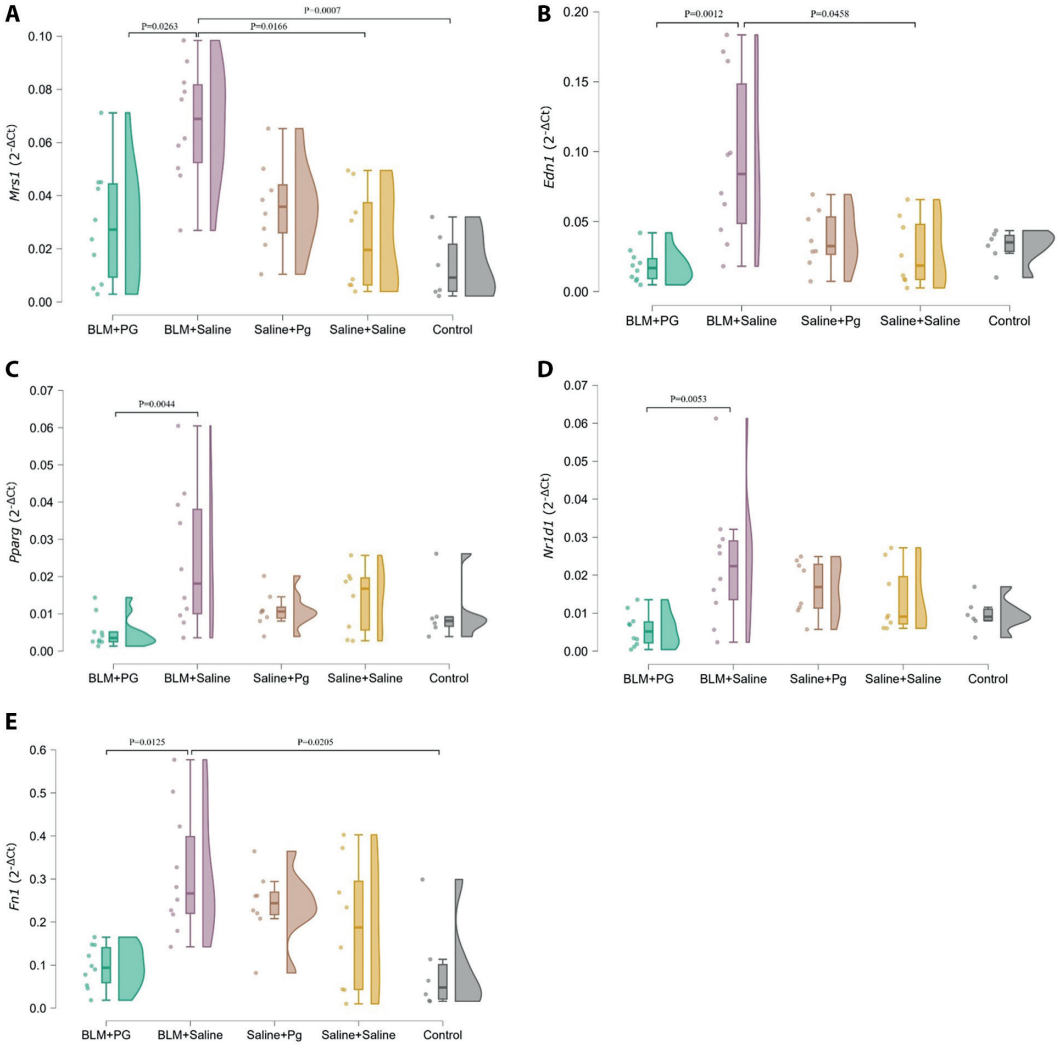

Figure 5. Changes in gene expression levels: A) *Mrc1*; B) *Edn1*; C) *Pparg*; D) *Nr1d1*; E) *Fn1*. Between-group differences were determined by one-way ANOVA with Tukey's *post hoc* test. The Kruskal-Wallis test was used to compare the Control group with all others. Exact P-values are given.

differences in 4-hydroxyproline concentration. This result reminds us to be cautious when using the 4-hydroxyproline content assay to evaluate the severity of lung fibrosis [51].

At the same time, we observed an increase in *Tgfb2* mRNA expression and *Tgfb3* mRNA expression (statistically insignificant). These TGF-beta isoforms drive the pathogenesis of fibrotic diseases, including lung fibrosis [52, 53].

Induction of BIF showed an increase in lung *Mrc1* mRNA expression. The *Mrc1* gene encodes the synthesis of macrophage scavenger receptor 1 (CD206). CD206-expressing M2 macrophages are involved in lung fibrosis progression [54]. Also, in lung fibrosis, the endothelin-1 played an important role in derived fibroblast activation, proliferation, as well as differentiation into myofibroblasts – processes that lead to excessive collagen deposition [55]. We also observed the increase of *Edn1* mRNA in mice lungs. Another potential contributor to lung fibrosis is fibronectin 1 (Fn1) [56], which might be involved together with collagen type 1 in airway remodeling [57]. In murine BIF, there was an increase in *Fn1* mRNA.

In our study, we estimated the mRNA expression of two important nuclear receptors, NR1D1 (Rev-Erb alpha) and PPAR-gamma, which have a wide range

of downstream target genes that are involved in many physiopathological processes, such as immunity, inflammation, autophagy, metabolism, etc. [24, 58]. After the BIF induction, a statistically insignificant increase in *Pparg* and *Nr1d1* mRNA was observed. This insignificance can be explained by the high individual variation of gene expression. We hypothesize that this slight increase of *Pparg* and *Nr1d1* mRNA might display the beginning of restorative processes in lung tissue on the 20th day after BIF induction. This suggestion goes in parallel with the observation of the importance of *Pparg* in the pathogenesis of lung fibrosis in other models [59] as well as *Nr1d1* [60]. It was shown that Rev-Erb alpha reduced PF by suppressing fibroblast differentiation [61]. Moreover, the absence of PPARG-associated ligands may have led to a compensatory increase in expression of their receptors [62].

Thus, the development of the BIF model led to an increase in collagen deposition, *Col1a1* and *Col3a1* mRNA expression with complicated lung tissue remodeling (*Mmp2*, *Edn1*, and *Fn1* mRNA overexpression), and *Mrc1* (CD206) mRNA expression (characterizing profibrotic M2 macrophages).

Administration of the PPARG agonist PG decreased collagen deposition, *Col1a1*, and *Col3a1* mRNA expression. At the same time, we observed the decreasing of *Tgfb2* and *Tgfb3* mRNA expression. *Mmp2* mRNA expression, as well as *Mrc1*, *Edn1*, and *Fn1*, were decreased after PG treatment. In addition, PG administration statistically significantly decreases the *Pparg* and *Nr1d1* mRNA expression up to the normal level. This observation needs further discussion. In the basal state, the PPAR-RXR complex is bound to corepressor and is transcriptionally inactive. The binding of different ligands promotes a conformational change, which results in the release of corepressors, allowing the recruitment of – and the interaction with coactivators [63]. It was shown that after PPARG stimulation, PPAR-RXR complex interacts with target genes and cell-type-specific coregulators, and this led to the decrease of *Pparg* expression [64, 65]. On the other hand, NR1D1 (Rev-Erb alpha) is an orphan nuclear receptor and is induced by PPARG activation [66]. These data support the idea of coordinated expression of *Pparg* and *Nr1d1* genes.

PG didn't have a statistical significant effect after saline exposure on the mRNA expression of *Col1a1*, *Col3a1*, *Mmp2*, *Mmp9*, *Tgfb2*, *Tgfb3* as well as *Mrc1*, *Edn1*, *Pparg*, *Nr1d1*, *Fn1* in healthy animals. These data go in parallel with observations that PG primarily acts to normalize increased tissue expression of profibrotic factors, rather than decrease basal (normal) expression in healthy tissues [67-71].

Thus, PG treatment alleviates the development of BIF through the activation of PPARG with consequent depression of TGF-beta/Smad pathways [72-74], which had an important role for procollagen 1A1, 3A1, and fibronectin synthesis [75]. In addition, PG prevented endothelin-1 mRNA expression during lung fibrosis. The endothelin-1 promotor recruits AP-1, HIF-1, and GATA2 [76], which counteract PPARG [77-79].

Our study has several limitations: 1) significant individual variability in the mRNA expression together with the limited number of animals per group may reduce the sensitivity of the study; 2) the future investigations on protein level are needed to prove antifibrotic and immunomodulative activity of PG, including cytokines and PPARG cofactors.

Conclusion

Activation of PPARG by PG alleviates BIF, decreasing collagen deposition, *Col1a1* and *Col3a1* mRNA expression, remodeling of lung tissue (decreasing *Mmp2*, *Edn1*, and *Fn1* mRNA), and M2-specific profibrotic macrophage *Mrc1* mRNA.

References

1. Stolz D, Mkorombindo T, Schumann DM, Agusti A, Ash SY, Bafadhel M, et al. Towards the elimination of chronic obstructive pulmonary disease: a Lancet Commission. Lancet 2022;400(10356):921-72.
2. Yang XY, Li F, Zhang G, Foster PS, Yang M. The role of macrophages in asthma-related fibrosis and remodelling. Pharmacol Ther 2025;269:108820.
3. Parimon T, Espindola M, Marchevsky A, Rampolla R, Chen P, Hogaboam CM. Potential mechanisms for lung fibrosis associated with COVID-19 infection. QJM 2023;116(7):487-92.

4. Muri J, Durcová B, Slivka R, Vrbenská A, Makovická M, Makovický P, et al. Idiopathic Pulmonary Fibrosis: Review of Current Knowledge. Physiol Res 2024;73(4):487-97.
5. Huo C, Jiao X, Wang Y, Jiang Q, Ning F, Wang J, et al. Silica aggravates pulmonary fibrosis through disrupting lung microbiota and amino acid metabolites. Sci Total Environ 2024;945:174028.
6. Xue S, Broerman MJ, Goobie GC, Kass DJ, Fabisiak JP, Wenzel SE, et al. Gaseous Air Pollutants and Lung Function in Fibrotic Interstitial Lung Disease (fILD): Evaluation of Different Spatial Analysis Approaches. Environ Sci Technol 2025;59(12):5936-45.
7. Weng C, Zhao Y, Song M, Shao Z, Pang Y, Yu C, et al. Mosaic loss of chromosome Y, tobacco smoking and risk of age-related lung diseases: insights from two prospective cohorts. Eur Respir J 2024;64(6):2400968.
8. Milman Krentsis I, Zheng Y, Rosen C, Shin SY, Blagdon C, Shoshan E, et al. Lung cell transplantation for pulmonary fibrosis. Sci Adv 2024;10(34):eadk2524.
9. George PM, Patterson CM, Reed AK, Thillai M. Lung transplantation for idiopathic pulmonary fibrosis. Lancet Respir Med 2019;7(3):271-82.
10. Fließer E, Jandl K, Lins T, Birnhuber A, Valzano F, Kolb D, et al. Lung Fibrosis Is Linked to Increased Endothelial Cell Activation and Dysfunctional Vascular Barrier Integrity. Am J Respir Cell Mol Biol 2024;71(3):318-31.
11. Khan MM, Galea G, Jung J, Zukowska J, Lauer D, Tuechler N, et al. Dextromethorphan inhibits collagen and collagen-like cargo secretion to ameliorate lung fibrosis. Sci Transl Med 2024;16(778):eadj3087.
12. Yadav P, Gómez Ortega J, Dabral P, Tamaki W, Chien C, Chang KC, et al. Myeloid-mesenchymal crosstalk drives ARG1-dependent profibrotic metabolism via ornithine in lung fibrosis. J Clin Invest 2025:e188734.
13. Wang J, Li K, Hao D, Li X, Zhu Y, Yu H, et al. Pulmonary fibrosis: pathogenesis and therapeutic strategies. MedComm (2020) 2024;5(10):e744.
14. Kamiya M, Carter H, Espindola MS, Doyle TJ, Lee JS, Merriam LT, et al. Immune mechanisms in fibrotic interstitial lung disease. Cell 2024;187(14):3506-30.
15. Alanazi FJ, Alruwaili AN, Aldhafeeri NA, Ballal S, Sharma R, Debnath S, et al. Pathological interplay of NF-κB and M1 macrophages in chronic inflammatory lung diseases. Pathol Res Pract 2025;269:155903.
16. Valenzi E, Jia M, Gerges P, Fan J, Tabib T, Behara R, et al. Altered AP-1, RUNX and EGR chromatin dynamics drive fibrotic lung disease. Preprint. bioRxiv 2024;2024.10.23.619858.
17. Wang Y, Zhao Y, Cao G, Jiang M, Yuan X, Li H, et al. STAT3 Facilitates Super Enhancer Formation to Promote Fibroblast-To-Myofibroblast Differentiation by the Analysis of ATAC-Seq, RNA-Seq and ChIP-Seq. J Cell Mol Med 2025;29(11):e70639.
18. Boateng E, Bonilla-Martinez R, Ahlemeyer B, Garikapati V, Alam MR, Trompak O, et al. It takes two peroxisome proliferator-activated receptors (PPAR-β/δ and PPAR-γ) to tango idiopathic pulmonary fibrosis. Respir Res 2024;25(1):345.
19. Pan X, Wang L, Yang J, Li Y, Xu M, Liang C, et al. TRβ activation confers AT2-to-AT1 cell differentiation and anti-fibrosis during lung repair via KLF2 and CEBPA. Nat Commun 2024;15(1):8672.
20. Wan R, Long S, Ma S, Yan P, Li Z, Xu K, et al. NR2F2 alleviates pulmonary fibrosis by inhibition of epithelial cell senescence. Respir Res 2024;25(1):154.
21. Wei A, Gao Q, Chen F, Zhu X, Chen X, Zhang L, et al. Inhibition of DNA methylation de-represses peroxisome proliferator-activated receptor-γ and attenuates pulmonary fibrosis. Br J Pharmacol 2022;179(7):1304-18.
22. Li G, Zhang Y, Jiang H, Wu X, Hao Y, Su Y, et al. PPARG/SPP1/CD44 signaling pathway in alveolar macrophages: Mechanisms of lipid dysregulation and therapeutic targets in idiopathic pulmonary fibrosis. Heliyon 2025;11(1):e41628.
23. Yang S, Sun Y, Luo Y, Liu Y, Jiang M, Li J, et al. Hypermethylation of PPARG-encoding gene promoter mediates fine particulate matter-induced pulmonary fibrosis by regulating the HMGB1/NLRP3 axis. Ecotoxicol Environ Saf 2024;272:116068.
24. Kökény G, Calvier L, Hansmann G. PPARγ and TGFβ-Major Regulators of Metabolism, Inflammation, and Fibrosis in the Lungs and Kidneys. Int J Mol Sci 2021; 22(19):10431.
25. Amin F, Memarzia A, Roohbakhsh A, Shakeri F, Boskabady MH. Zataria multiflora and Pioglitazone Affect Systemic Inflammation and Oxidative Stress Induced by Inhaled Paraquat in Rats. Mediators Inflamm 2021;2021:5575059.
26. Legchenko E, Chouvarine P, Borchert P, Fernandez-Gonzalez A, Snay E, Meier M, et al. PPARγ agonist pioglitazone reverses pulmonary hypertension and prevents right heart failure via fatty acid oxidation. Sci Transl Med 2018;10(438):eaao0303.
27. Kurihara C, Sakurai R, Chuang TD, Waring AJ, Walther FJ, Rehan VK. Combination of pioglitazone, a PPARγ agonist, and synthetic surfactant B-YL prevents hyperoxia -induced lung injury in adult mice lung explants. Pulm Pharmacol Ther 2023;80:102209.
28. Tang J, Dong W, Wang D, Deng Q, Guo H, Xiao G. Upregulation of PGC-1α expression by pioglitazone mediates prevention of sepsis-induced acute lung injury. Braz J Med Biol Res 2024;57:e13235.
29. Yeligar SM, Mehta AJ, Harris FL, Brown LAS, Hart CM. Pioglitazone Reverses Alcohol-Induced Alveolar Macrophage Phagocytic Dysfunction. J Immunol 2021;207(2):483-92.
30. Huang T, Lin R, Su Y, Sun H, Zheng X, Zhang J, et al. Efficient intervention for pulmonary fibrosis via mitochondrial transfer promoted by mitochondrial biogenesis. Nat Commun 2023;14(1):5781.
31. Schrier DJ, Phan SH. Modulation of bleomycin-induced pulmonary fibrosis in the BALB/c mouse by cyclophosphamide -sensitive T cells. Am J Pathol 1984;116(2):270-8.

32. Egger C, Cannet C, Gérard C, Jarman E, Jarai G, Feige A, et al. Administration of bleomycin via the oropharyngeal aspiration route leads to sustained lung fibrosis in mice and rats as quantified by UTE-MRI and histology. PLoS One 2013;8(5):e63432.
33. Kabaley A, Izmailova O, Palchyk V, Shinkevich, V, Shlykova O. The PPARG receptor agonist pioglitazone reduces the manifestations of pulmonary fibrosis in mice induced by bleomycin administration. Med and Ecol probl 2024;28(3):19-27.
34. Shlykova O, Izmailova O, Kabaliei A, Palchyk V, Shynkevych V, Kaidashev I. PPARG stimulation restored lung mRNA expression of core clock, inflammation- and metabolism-related genes disrupted by reversed feeding in male mice. Physiol Rep 2023;11(17):e15823.
35. Van Hoecke L, Job ER, Saelens X, Roose K. Bronchoalveolar lavage of murine lungs to analyze inflammatory cell infiltration. J Vis Exp 2017;(123):55398.
36. Piccinini F, Tesei A, Arienti C, Bevilacqua A. Cell counting and viability assessment of 2D and 3D cell cultures: expected reliability of the Trypan Blue assay. Biol Proced Online 2017:19:8.
37. Memon MA, Anway MD, Covert TR, Uzumcu M, Skinner MK. Transforming growth factor beta (TGFbeta1, TGFbeta2 and TGFbeta3) null-mutant phenotypes in embryonic gonadal development. Mol Cell Endocrinol 2008;294(1-2):70-80.
38. Lu J, Xie L, Liu C, Zhang Q, Sun S. PTEN/PI3k/AKT Regulates Macrophage Polarization in Emphysematous mice. Scand J Immunol 2017;85(6):395-405.
39. Neder TH, Schrankl J, Fuchs MAA, Broeker KAE, Wagner C. Endothelin receptors in renal interstitial cells do not contribute to the development of fibrosis during experimental kidney disease. Pflugers Arch 2021;473(10):1667-83.
40. Ke L, Yang Y, Li JW, Wang B, Wang Y, Yang W, et al. Modulation of Corneal FAK/PI3K/Akt Signaling Expression and of Metalloproteinase-2 and Metalloproteinase-9 during the Development of Herpes Simplex Keratitis. Biomed Res Int 2019;2019:4143981.
41. Kabaliei A, Palchyk V, Izmailova O, Shynkevych V, Shlykova O, Kaidashev I. Long-term administration of Omeprazole-induced hypergastrinemia and changed glucose homeostasis and expression of metabolism-related genes. Biomed Res Int 2024;2024:7747599.
42. Liu S, Cai Y, Sothern RB, Guan Y, Chan P. Chronobiological analysis of circadian patterns in transcription of seven key clock genes in six peripheral tissues in mice. Chronobiol Int 2007;24(5):793-820.
43. Masugi Y, Abe T, Tsujikawa H, Effendi K, Hashiguchi A, Abe M, et al. Quantitative assessment of liver fibrosis reveals a nonlinear association with fibrosis stage in nonalcoholic fatty liver disease. Hepatol Commun 2017;2(1):58-68.
44. Moore BB, Hogaboam CM. Murine models of pulmonary fibrosis. Am J Physiol Lung Cell Mol Physiol 2008;294(2):L152-L160.
45. Adamcakova J, Palova R, Mokra D. Experimental models of pulmonary fibrosis and their translational potential. Acta Medica Martiniana 2019;19(3):95-102.
46. Li X, Sun X, Kan C, Chen B, Qu N, Hou N, et al. COL1A1: A novel oncogenic gene and therapeutic target in malignancies. Pathol Res Pract 2022;236:154013.
47. Lin Y, Li Y, Chen P, Zhang Y, Sun J, Sun X, et al. Exosome-based regimen rescues endometrial fibrosis in intrauterine adhesions via targeting clinical fibrosis biomarkers. Stem Cells Transl Med 2023;12(3):154-68.
48. Chen P, Xie L, Ma L, Zhao X, Chen Y, Ge Z. Prediction and analysis of genetic effect in idiopathic pulmonary fibrosis and gastroesophageal reflux disease. IET Syst Biol 2023;17(6):352-65.
49. Wang R, Wu G, Dai T, Lang Y, Chi Z, Yang S, et al. Naringin attenuates renal interstitial fibrosis by regulating the TGF-β/Smad signaling pathway and inflammation. Exp Ther Med 2021;21(1):66.
50. Zhao J, Yu W, Zhou D, Liu Y, Wei J, Bi L, et al. Delineating, imaging, and assessing pulmonary fibrosis remodeling via collagen hybridization. ACS Nano 2024;18(41): 27997-28011.
51. Song S, Fu Z, Guan R, Zhao J, Yang P, Li Y, et al. Intracellular hydroxyproline imprinting following resolution of bleomycin-induced pulmonary fibrosis. Eur Respir J 2022;59(5):2100864.
52. Sun T, Huang Z, Liang WC, Yin J, Lin WY, Wu J, et al. TGFβ2 and TGFβ3 isoforms drive fibrotic disease pathogenesis. Sci Transl Med 2021;13(605):eabe0407.
53. Duan FF, Barron G, Meliton A, Mutlu GM, Dulin NO, Schuger L. P311 promotes lung fibrosis via stimulation of transforming growth factor-β1, -β2, and -β3 translation. Am J Respir Cell Mol Biol 2019;60(2):221-31.
54. Pommerolle L, Beltramo G, Biziorek L, Truchi M, Dias AMM, Dondaine L, et al. CD206^{+} macrophages are relevant non-invasive imaging biomarkers and therapeutic targets in experimental lung fibrosis. Thorax 2024;79(12): 1124-35.
55. Swigris JJ, Brown KK. The role of endothelin-1 in the pathogenesis of idiopathic pulmonary fibrosis. BioDrugs 2010;24(1):49-54.
56. Alsafadi HN, Staab-Weijnitz CA, Lehmann M, Lindner M, Peschel B, Königshoff M, et al. An ex vivo model to induce early fibrosis-like changes in human precision-cut lung slices. Am J Physiol Lung Cell Mol Physiol. 2017;312(6):L896-L902. Erratum in: Am J Physiol Lung Cell Mol Physiol 2020;318(4):L844.
57. Guo Z, Wu J, Zhao J, Liu F, Chen Y, Bi L, et al. [IL-33 /ST2 promotes airway remodeling in asthma by activating the expression of fibronectin 1 and type 1 collagen in human lung fibroblasts]. Xi Bao Yu Fen Zi Mian Yi Xue Za Zhi 2014;30(9):975-9.
58. Zhang-Sun ZY, Xu XZ, Escames G, Lei WR, Zhao L, Zhou YZ, et al. Targeting NR1D1 in organ injury: challenges and prospects. Mil Med Res 2023;10(1):62.

59. Malur A, Mohan A, Barrington RA, Leffler N, Malur A, Muller-Borer B et al. Peroxisome proliferator-activated receptor-γ deficiency exacerbates fibrotic response to mycobacteria peptide in murine sarcoidosis model. Am J Respir Cell Mol Biol 2019;61(2):198-208.
60. Zhao Z, Shan X, Ding J, Ma B, Li B, Huang W, et al. Boosting RNA nanotherapeutics with V-ATPase activating non-inflammatory lipid nanoparticles to treat chronic lung injury. Nat Commun 2025;16(1):6477.
61. Raza GS, Sodum N, Kaya Y, Herzig KH. Role of circadian transcription factor Rev-Erb in metabolism and tissue fibrosis. Int J Mol Sci 2022;23(21):12954.
62. Esmaeili S, Salari S, Kaveh V, Ghaffari SH, Bashash D. Alteration of PPAR-GAMMA (PPARG; PPARγ) and PTEN gene expression in acute myeloid leukemia patients and the promising anticancer effects of PPARγ stimulation using pioglitazone on AML cells. Mol Genet Genomic Med 2021;9(11):e1818.
63. Costa V, Gallo MA, Letizia F, Aprile M, Casamassimi A, Ciccodicola A. PPARG: gene expression regulation and next-generation sequencing for unsolved issues. PPAR Res 2010;2010:409168.
64. Nielsen R, Pedersen TA, Hagenbeek D, Moulos P, Siersbaek R, Megens E, et al. Genome-wide profiling of PPARgamma: RXR and RNA polymerase II occupancy reveals temporal activation of distinct metabolic pathways and changes in RXR dimer composition during adipogenesis. Genes Dev 2008;22(21):2953-67.
65. Lefterova MI, Steger DJ, Zhuo D, Qatanani M, Mullican SE, Tuteja G, et al. Cell-specific determinants of peroxisome proliferator-activated receptor gamma function in adipocytes and macrophages. Mol Cell Biol 2010;30(9):2078-89.
66. Fontaine C, Dubois G, Duguay Y, Helledie T, Vu-Dac N, Gervois P, et al. The orphan nuclear receptor Rev-Erbalpha is a peroxisome proliferator-activated receptor (PPAR) gamma target gene and promotes PPARgamma-induced adipocyte differentiation. J Biol Chem 2003;278(39): 37672-80.
67. Levine B. Eating oneself and uninvited guests: autophagy-related pathways in cellular defense. Cell. 2005;120(2):159-162.
68. Manzéger A, Garmaa G, Mózes MM, Hansmann G, Kökény G. Pioglitazone Protects Tubular Epithelial Cells during Kidney Fibrosis by Attenuating miRNA Dysregulation and Autophagy Dysfunction Induced by TGF-β. Int J Mol Sci 2023;24(21):15520.
69. Gao D, Ning N, Hao G, Niu X. Pioglitazone attenuates vascular fibrosis in spontaneously hypertensive rats. PPAR Res. 2012;2012:856426.
70. Zhang J, Huang X, Wang L. Pioglitazone inhibits the expression of matrix metalloproteinase-9, a protein involved in diabetes-associated wound healing. Mol Med Rep 2014;10(2):1084-1088.
71. Aluru S, Thyagarajan A, Sahu RP. Pioglitazone-Based Combination Approaches for Non-Small-Cell Lung Cancer. Pharmaceutics 2025;17(11):1416.
72. Serizawa M, Murakami H, Watanabe M, Takahashi T, Yamamoto N, Koh Y. Peroxisome proliferator-activated receptor γ agonist efatutazone impairs transforming growth factor β2-induced motility of epidermal growth factor receptor tyrosine kinase inhibitor-resistant lung cancer cells. Cancer Sci 2014;105(6):683-9.
73. Redondo S, Hristov M, Gümbel D, Tejerina T, Weber C. Biphasic effect of pioglitazone on isolated human endothelial progenitor cells: involvement of peroxisome proliferator -activated receptor-gamma and transforming growth factor -beta1. Thromb Haemost 2007;97(6):979-87.
74. Yu Q, Cheng P, Wu J, Guo C. PPARγ/NF-κB and TGF-β1/Smad pathway are involved in the anti-fibrotic effects of levo-tetrahydropalmatine on liver fibrosis. J Cell Mol Med 2021;25(3):1645-60.
75. Koo JB, Nam MO, Jung Y, Yoo J, Kim DH, Kim G, et al. Anti-fibrogenic effect of PPAR-γ agonists in human intestinal myofibroblasts. BMC Gastroenterol 2017;17(1):73.
76. Stow LR, Jacobs ME, Wingo CS, Cain BD. Endothelin-1 gene regulation. FASEB J 2011;25(1):16-28.
77. Yun Z, Maecker HL, Johnson RS, Giaccia AJ. Inhibition of PPAR gamma 2 gene expression by the HIF-1-regulated gene DEC1/Stra13: a mechanism for regulation of adipogenesis by hypoxia. Dev Cell 2002;2(3):331-41.
78. Xu Y, Takahashi Y, Wang Y, Hama A, Nishio N, Muramatsu H, et al. Downregulation of GATA-2 and overexpression of adipogenic gene-PPARgamma in mesenchymal stem cells from patients with aplastic anemia. Exp Hematol 2009;37(12):1393-9.
79. Carvalho MV, Gonçalves-de-Albuquerque CF, Silva AR. PPAR Gamma: From Definition to Molecular Targets and Therapy of Lung Diseases. Int J Mol Sci 2021;22(2):805.

Received for publication: 29 October 2025 - Accepted for publication: 3 March 2026

Licensee Mattioli 1885, Italy
Multidisciplinary Respiratory Medicine 2026; 21: 1068
doi: 10.5826/mrm.2026.1068